

UC Davis

UC Davis Previously Published Works

Title

Time- and region-dependent blood-brain barrier impairment in a rat model of organophosphate-induced status epilepticus

Permalink

<https://escholarship.org/uc/item/8r04b5nm>

Authors

Bernardino, Pedro N

Hobson, Brad A

Huddleston, Sydney L

et al.

Publication Date

2023-10-01

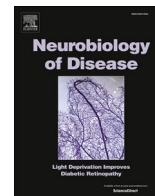
DOI

10.1016/j.nbd.2023.106316

Copyright Information

This work is made available under the terms of a Creative Commons Attribution-NoDerivatives License, available at <https://creativecommons.org/licenses/by-nd/4.0/>

Peer reviewed



Time- and region-dependent blood-brain barrier impairment in a rat model of organophosphate-induced status epilepticus

Pedro N. Bernardino^a, Brad A. Hobson^b, Sydney L. Huddleston^b, Peter M. Andrew^a, Jeremy A. MacMahon^a, Naomi H. Saito^c, Valerie A. Porter^d, Donald A. Bruun^a, Danielle J. Harvey^c, Joel R. Garbow^e, Angie Gelli^f, Abhijit J. Chaudhari^{b,g}, Pamela J. Lein^{a,*}

^a Department of Molecular Biosciences, University of California, Davis, School of Veterinary Medicine, Davis, CA 95616, USA

^b Center for Molecular and Genomic Imaging, University of California, Davis, Davis, CA 95616, USA

^c Department of Public Health Sciences, University of California, Davis, School of Medicine, Davis, CA 95616, USA

^d Department of Biomedical Engineering, University of California, Davis, College of Engineering, Davis, CA 95616, USA

^e Biomedical Magnetic Resonance Center, Mallinckrodt Institute of Radiology, School of Medicine, Washington University in St. Louis, St. Louis, MO 63110, USA

^f Department of Pharmacology, University of California, Davis, School of Medicine, Davis, CA 95616, USA

^g Department of Radiology, University of California, Davis, School of Medicine, Sacramento, CA 95817, USA

ARTICLE INFO

Keywords:

Albumin
Blood-brain barrier impairment
Diisopropylfluorophosphate
Epilepsy
MRI
Organophosphate
Spontaneous recurrent seizures

ABSTRACT

Acute organophosphate (OP) intoxication can trigger seizures that progress to status epilepticus (SE), and survivors often develop chronic morbidities, including spontaneous recurrent seizures (SRS). The pathogenic mechanisms underlying OP-induced SRS are unknown, but increased BBB permeability is hypothesized to be involved. Previous studies reported BBB leakage following OP-induced SE, but key information regarding time and regional distribution of BBB impairment during the epileptogenic period is missing. To address this data gap, we characterized the spatiotemporal progression of BBB impairment during the first week post-exposure in a rat model of diisopropylfluorophosphate-induced SE, using MRI and albumin immunohistochemistry. Increased BBB permeability, which was detected at 6 h and persisted up to 7 d post-exposure, was most severe and persistent in the piriform cortex and amygdala, moderate but persistent in the thalamus, and less severe and transient in the hippocampus and somatosensory cortex. The extent of BBB leakage was positively correlated with behavioral seizure severity, with the strongest association identified in the piriform cortex and amygdala. These findings provide evidence of the duration, magnitude and spatial breakdown of the BBB during the epileptogenic period following OP-induced SE and support BBB regulation as a viable therapeutic target for preventing SRS following acute OP intoxication.

1. Introduction

Acute intoxication with organophosphate (OP) cholinesterase inhibitors as a result of accidental or intentional exposure affects millions of people each year (Bird et al., 2014; Jett et al., 2020; Mew et al., 2017). The cholinergic crisis resulting from acute OP intoxication can trigger seizures that rapidly progress to status epilepticus (SE) (Eddleston et al., 2008). Benzodiazepines are the first-line treatment for OP-induced SE, with current guidelines recommending administration within 5–10 min

of seizure onset. Administration of standard of care within 5–10 min of seizure initiation is unrealistic in most scenarios of acute OP intoxication in humans (Hill et al., 2017; Kapur et al., 2019), imposing a significant limitation on effective management of OP-induced SE. Additionally, the current standard of care for acute OP intoxication does not protect against ensuing brain injury and the development of spontaneous recurrent seizures (SRS) (Waheed et al., 2014) and other neurological morbidities (Jh et al., 2000; Masson, 2011; Shih, 1990; Weissman and Raveh, 2008). The general lack of understanding of the pathogenic

* Corresponding author at: Molecular Biosciences, UC Davis School of Veterinary Medicine, 1089 Veterinary Research Drive, Davis, CA 95616, USA.

E-mail addresses: pberna@ucdavis.edu (P.N. Bernardino), bahobson@ucdavis.edu (B.A. Hobson), slhuddleston@ucdavis.edu (S.L. Huddleston), pandrew@ucdavis.edu (P.M. Andrew), jamacmahon@ucdavis.edu (J.A. MacMahon), nhsaito@ucdavis.edu (N.H. Saito), vporter@ucdavis.edu (V.A. Porter), dabruun@ucdavis.edu (D.A. Bruun), djharvey@ucdavis.edu (D.J. Harvey), garbow@wustl.edu (J.R. Garbow), agelli@ucdavis.edu (A. Gelli), ajchaudhari@ucdavis.edu (A.J. Chaudhari), pjlein@ucdavis.edu (P.J. Lein).

<https://doi.org/10.1016/j.nbd.2023.106316>

Received 2 May 2023; Received in revised form 26 September 2023; Accepted 2 October 2023

Available online 4 October 2023

0969-9961/© 2023 The Authors. Published by Elsevier Inc. This is an open access article under the CC BY-NC-ND license (<http://creativecommons.org/licenses/by-nc-nd/4.0/>).

mechanisms that link OP-induced SE to neurological sequelae has significantly stymied the development of therapies against those morbidities, including therapies that could be administered at delayed times post-OP exposure.

Several lines of evidence suggest that protecting blood-brain barrier (BBB) integrity following acute OP intoxication may be an effective therapeutic strategy for preventing or reducing SRS. The BBB is essential for maintaining brain homeostasis (Abbott et al., 2010; Kadry et al., 2020). BBB impairment is linked to poor outcomes following stroke and traumatic brain injury, and to the progression of neurodegenerative disease (Profaci et al., 2020). Clinical and experimental evidence also implicate BBB impairment in the pathogenesis of epilepsy (Li et al., 2023; Marchi et al., 2012; van Lanen et al., 2021; Van Vliet et al., 2015). In patients with epilepsy, increased BBB permeability is associated with progressive neurodegeneration and signs of cognitive and behavioral impairment (Farrell et al., 2017; Uprety et al., 2021). In SE, impaired BBB integrity may be an early biomarker of cognitive impairment and has been associated with the development and progression of acquired epilepsy in both humans and animal models of SE caused by factors other than acute OP intoxication (Bar-Klein et al., 2017; Dadas and Janigro, 2019; Mendes et al., 2019; Nation et al., 2019; Tenreiro et al., 2016).

To date, few studies have evaluated BBB integrity after acute OP intoxication, and of those that have, all reported evidence of BBB impairment following OP-induced SE. In animal models of acute intoxication with the OPs sarin (Abdel-Rahman et al., 2002), soman (Rojas et al., 2021), diisopropylfluorophosphate (DFP) (Rojas et al., 2022; Rojas et al., 2021) or paraoxon (Bar-Klein et al., 2017), BBB breakdown was observed as early as 3 h post-exposure (Rojas et al., 2022) and as late as 1 month post-exposure (Bar-Klein et al., 2017). One of these preclinical studies (Bar-Klein et al., 2017) also showed that isoflurane anesthesia or losartan were effective in preventing both early microvascular damage and the onset of SRS when administered 30 min after acute intoxication with paraoxon. While these studies suggest that protecting BBB integrity may be efficacious in mitigating or preventing SRS in individuals acutely intoxicated with OPs, they each have significant limitations. First, temporal progression of BBB impairment remains unclear due to lack of longitudinal analyses or comparison across times post-exposure. Second, in three of the four studies, the BBB was assessed using techniques that do not provide refined spatial data regarding BBB impairment, e.g., western blot analysis of serum albumin in brain parenchyma (Rojas et al., 2022; Rojas et al., 2021) or [³H] hexamethonium iodide uptake (Abdel-Rahman et al., 2002). The one study (Bar-Klein et al., 2017) that used in vivo imaging to assess BBB integrity scanner and imaging parameters with limited signal to noise ratio and relied on spatial averaging, which decreased spatial resolution, and histological confirmation of BBB leakage was observed in only one of the regions (piriform cortex). Third, in two studies, the standard anti-seizure medication was never administered (Abdel-Rahman et al., 2002; Rojas et al., 2022), while the other two used models in which OP-induced SE was pharmacologically terminated with agents other than benzodiazepines at 30 or 60 min post-exposure (Bar-Klein et al., 2017; Rojas et al., 2021). None of those scenarios replicate the more typical human experience of delayed benzodiazepine administration at ≥ 30 min after SE onset (Hill et al., 2017), with minimal impact on seizure activity. Therefore, detailed characterization of the duration, magnitude, and spatial distribution of BBB dysfunction in a preclinical model that closely recapitulates the human experience of prolonged seizure activity following acute OP intoxication, even after standard of care, is lacking. These data would support studies of BBB impairment as an underlying mechanism leading to OP-induced SE.

We previously demonstrated that rats acutely intoxicated with DFP experience SE for hours despite being treated at 40 min post-exposure with the human-equivalent dose of the benzodiazepine, midazolam (Supasai et al., 2020). Here, we generated a spatiotemporal map of BBB impairment in a similar model (without administration of

pyridostigmine bromide) using contrast-enhanced MRI (CE-MRI), which is the current standard for evaluating BBB integrity in the clinical setting, and ex vivo albumin immunohistochemistry (IHC). In animal models of acute intoxication with soman or paraoxon, SRS manifested in the majority of surviving animals within 5–10 days post-exposure (De Araujo Furtado et al., 2010; de Araujo Furtado et al., 2012; Shrot et al., 2014). Consistent with these observations, our pilot studies of the rat model of acute DFP intoxication suggested that SRS developed in DFP-intoxicated rats within 5–7 days post-exposure (Guignet et al., 2020). Since our long-term objective is to determine whether therapeutic strategies aimed at preventing or mitigating BBB breakdown following OP-induced SE are effective in blocking acquired epilepsy, BBB leakage was quantified at 6 h, 1 d, 3 d and 7 d post-exposure. Here, we demonstrate that DFP-induced SE caused significant time- and region-dependent BBB impairment in the rat brain when standard of care was administered at delayed times.

2. Materials and methods

2.1. Study approval

This study followed protocols approved by the UC Davis Institutional Animal Care and Use Committee (IACUC protocol number 21954) and used facilities fully accredited by AAALAC International. All experimentation was in accordance with the ARRIVE guidelines and the National Institute of Health (NIH) Guide for The Care and Use of Laboratory Animals (NIH publication No. 8023, revised 1978).

2.2. Study design

The primary objective of this study was to characterize the spatio-temporal pattern of BBB impairment during the first week after acute DFP intoxication with the long-term objective of identifying the therapeutic window for targeting BBB dysfunction to mitigate chronic adverse neurological sequelae. BBB impairment was evaluated using two different methods, MRI and albumin IHC at 6 h post-exposure (hPE), and 1, 3 and 7 d post-exposure (DPE). Sample size was calculated using the estimated effect size between DFP and vehicle (VEH) groups based on pilot studies of acutely-intoxicated DFP rats. The minimal number of animals per group needed to detect at least a 50% difference between groups with 80% power, assuming $\alpha = 0.05$ for a two-sided test was used. Adult male Sprague-Dawley rats, 250–300 g, were purchased from Charles Rivers Laboratories (Hollister, CA, USA), and after DFP exposure, survivors were randomly assigned to tissue collection endpoints using a random number generator. Animals that did not survive acute DFP intoxication were not included in the study. Rats were individually housed in standard plastic cages under controlled environment conditions (22 ± 2 °C, 40–50% humidity and 12 h light/dark cycle) and provided with food and water ad libitum. Study personnel were blinded to treatment group when quantifying MRI and albumin IHC data.

2.3. Materials

The purity of DFP (Sigma Chemical Company, St Louis, MO, USA) was determined to be $90 \pm 7\%$ using ¹H-, ¹³C-, ¹⁹F-, and ³¹P NMR, as described previously (Gao et al., 2016). DFP was aliquoted and stored at -80 °C, conditions under which it remains stable for 1 year (Heiss et al., 2016). Atropine sulfate and 2-pralidoxime (2-PAM) were obtained from Sigma and pharmaceutical grade midazolam (MDZ) from West-Ward Pharmaceuticals (Eatontown, NJ, USA). Certification of analysis provided by the manufacturers confirmed the purity of these three reagents was $\geq 97\%$.

2.4. Dosing paradigm and experimental design

As shown in Fig. 1A, rats were injected s.c. with DFP (4 mg/kg)

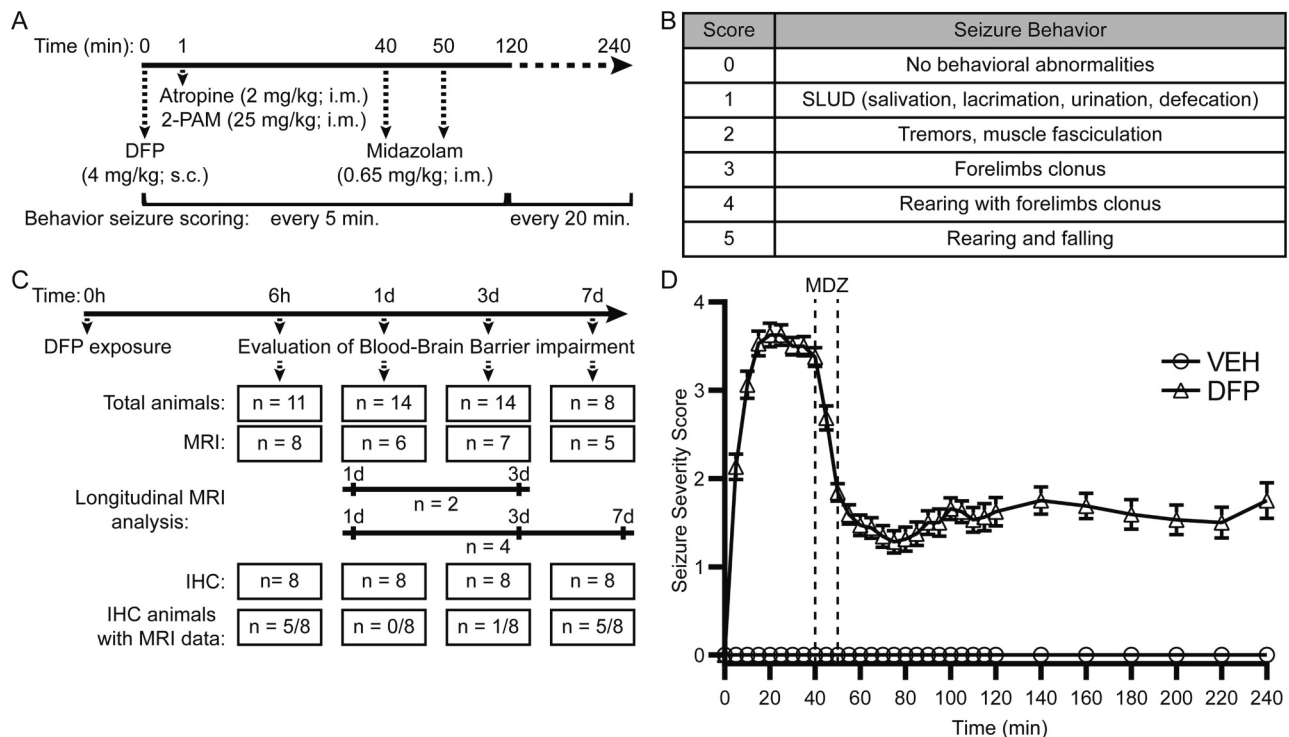


Fig. 1. Study design and seizure behavior following acute intoxication with diisopropylfluorophosphate (DFP). (A) Adult male Sprague Dawley rats were injected with DFP and immediately treated with atropine sulfate and 2-pralidoxime (2-PAM) followed by administration of midazolam (MDZ) at 40- and 50-min post-exposure. (B) Modified Racine Scale used to score seizure behavior during the first 4 h post-exposure (hPE). (C) 37 animals acutely intoxicated with DFP were included in the analyses of BBB impairment (vehicles not included in this diagram). Sixteen rats underwent MRI analyses of BBB impairment: 8 were evaluated at 6 hPE and brain was collected from 5 of them, while 3 animals died immediately after the procedure, excluding brain collection for IHC in those due to post-mortem alterations. Another 6 animals were evaluated longitudinally: 4 of them at 1, 3, and 7 DPE, followed by brain collection for IHC; and 2 of them at 1, and 3 DPE, with no brain collection due to death immediately after image acquisition. One animal was evaluated by MRI only at 3 DPE, and another at 7 DPE, both followed by brain collection for IHC. Twenty one rats were not evaluated by MRI, but had their brain collected at 6 hPE ($n = 3$), 1 DPE ($n = 8$), 3 DPE ($n = 7$), or 7 DPE ($n = 3$) for IHC evaluation of BBB impairment (D) Animals included in the DFP group of this study ($n = 37$) reached and maintained behavior seizure scores ≥ 3 until administered midazolam (MDZ), when the average seizure scores decreased to ≤ 2 ; animals in the vehicle (VEH; $n = 22$) group were always at 0 average seizure score. Data points correspond to the mean seizure score (\pm S.E.M.) at each observation time.

diluted in cold phosphate-buffered saline (PBS; 3.6 mM Na_2HPO_4 , 1.4 mM NaH_2PO_4 , 150 mM NaCl; pH 7.2) prepared within 5 min before injection. Control animals (VEH) were injected with an equal volume (300 μL) of PBS. To increase survival rate following DFP exposure, animals were injected within 1 min after DFP intoxication with atropine sulfate (2 mg/kg, i.m.) and 2-PAM (25 mg/kg, i.m.) in sterile isotonic saline (0.9% NaCl) (Bruun et al., 2019). At 40 and 50 min post-DFP, MDZ (0.65 mg/kg, i.m.) was administered. Two injections of MDZ were provided to replicate the current standard of care for OP-induced seizures (U.S Department of Health and Human Services. Nerve Agents, 2023), and the dose of 0.65 mg/kg, i.m., was previously predicted to produce serum C_{max} values in the rat similar to predicted C_{max} values in humans when the recommended dosing paradigm is followed (Dhir et al., 2021). VEH animals were similarly treated with atropine, 2-PAM and MDZ. Seizure behavior was scored during the initial 240 min using a modified Racine scale (Deshpande et al., 2016) (Fig. 1B). Only rats with an average seizure score of 2.5 or higher during the first 40 min post-DFP were included in this study. After 240 min, DFP animals received 10 mL, s.c., of Ringer's lactate with 5% dextrose (Baxter Healthcare Corporation, Deerfield, IL, USA) with repeated administration for 1–3 d until animals started to regain weight. Moist chow was provided in their home cage until they resumed consumption of solid chow.

2.5. MRI

Isoflurane gas (Western Medical Supply, Arcadia, CA, USA) was used

to induce and maintain anesthesia in rats undergoing MRI. Scans were performed using a Bruker Biospec 70/30 (7 T) preclinical MR scanner running Paravision 6.0 (Bruker BioSpin MRI, Ettlingen, Germany), equipped with a 116-mm internal diameter B-GA12S gradient (450 mT/m, 4500 T/m/s), a 72-mm internal diameter linear transmit coil, and a four-channel, rat-brain phased array in cross coil configuration for signal reception. Pre-contrast, high-resolution, multi-slice, T_1 -weighted (T_1w), Rapid Acquisition with Repeated Echoes (RARE) axial images were acquired using the following imaging parameters: repetition time (TR) = 700 ms; echo time (TE) = 7 ms; RARE factor = 2; averages = 10; field of view (FOV) = $30 \times 30 \text{ mm}^2$, with an in-plane data matrix of 240×240 , resulting in a data set resolution of $0.125 \times 0.125 \text{ mm}^2$; 27 slices with a 0.5 mm thickness spanning approximately 3.5 to -9.0 bregma. DCE images were acquired using the following imaging parameters: TR = 700 ms; TE = 7 ms; RARE factor = 2; averages = 4; FOV = $30 \times 30 \text{ mm}^2$, with an in-plane data matrix of 120×120 , resulting in a data set resolution of $0.250 \times 0.250 \text{ mm}^2$; and 27 slices with a 0.5 mm thickness centered in the middle of the pre-contrast T_1w FOV. DCE data were collected during 11 time frames over 23 m 6 s, with a temporal resolution of 126 s. At the start of the third DCE frame, 0.2 M Gd (gadobenate dimeglumine, Multihance®, Bracco Diagnostics Inc., Princeton, NJ, USA), diluted in 0.9% NaCl (Fresenius Kabi AG, Bad Homburg, Germany) was administered as a step-down infusion via tail-vein catheter connected to a programmable syringe pump (Braintree Scientific, Braintree, MA, USA). This protocol has been previously shown to produce high levels of steady-state circulating contrast agent needed to detect BBB impairment following SE (Van Vliet et al., 2014). At the

conclusion of the DCE scan, a post-contrast, high-resolution T₁w RARE scan was acquired using the same parameters as the pre-contrast scan. Total scan duration was approximately 60 min and included a T₂-weighted scan that is the subject of a separate manuscript and will not be discussed further herein.

For regional image analysis, volumes of interest (VOIs) were manually segmented on T₁w pre-contrast images to minimize the visual appearance of lesions that could bias segmentation (Fig. S1). Brain-region VOIs included: piriform cortex (PRC), amygdala (AMY), hippocampus (HIP), thalamus (THA; medial and dorsolateral), and somatosensory cortex (SMC). Image segmentation was performed in AMIRA 6.0 software (Thermo Fisher Scientific, Waltham, MA, USA) using Paxinos and Watson's *The Rat Brain in Stereotaxic Coordinates* (Paxinos and Watson, 2006) as a guide for anatomical boundaries. Parametric maps of Gd-infiltration (assessed as percent change between pre- and post-contrast T₁w image volumes), voxel-wise metric data, and regional analyses were generated in PMOD 4.3 (PMOD Technologies, Zurich, CHE). For each region, Gd-infiltration into brain parenchyma was assessed using the following metrics: 1) region-specific mean and standard deviation percent change in signal intensity, 2) number of voxels exceeding a threshold of 15% change in signal intensity, image intensity slopes, and 3) area under the signal intensity curve (AUC) across DCE frames.

2.6. Albumin IHC

Rats were anesthetized with 5% isoflurane in medical grade oxygen followed by perfusion with cold PBS (15 mL/min) using a Masterflex peristaltic pump (Cole Parmer, Vernon Hills, IL, USA). The brain was rapidly collected and bisected into the two hemispheres. One hemisphere was cut into 2-mm thick coronal sections using a stainless-steel small rat brain matrix (Zivic Instruments, Pittsburgh, PA, USA). Coronal sections were post-fixed in 4% (w/v) paraformaldehyde (Sigma) for 24 h, then equilibrated in 30% (w/v) sucrose (Thermo Fisher, Waltham, MA, USA) in ultrapure water for 72 h. Fixed sections were embedded in Optimal Cutting Temperature (OCT) medium (Thermo Fisher) and stored at -80 °C. Blocks were subsequently cryosectioned at 10 μm from bregma -3.3 to -4.2 onto Superfrost Plus Slides (Thermo Fisher) and stored at -20 °C until immunostained. A description of the immunostaining process and the antibody specifications can be found in the Supplemental Method section and in Supplemental Table 8. Two technical replicates were processed for each animal.

Images of the whole brain hemisphere were acquired at 10× magnification using the high-content ImageXpress XL imaging system (Molecular Devices, Sunnyvale, CA, USA) and analyzed using AMIRA 6.0 software (Thermo Fisher). Regions of interest drawn in AMIRA included: piriform cortex (PRC), amygdala (AMG), hippocampus (HIP), thalamus (THA), somatosensory cortex (SMC), and a reference region (sub-thalamic region identified as *Zona Incerta*; Fig. S1). The mean pixel intensity for albumin immunofluorescence was calculated for each region. The percent area of albumin immunoreactivity within each region was calculated as $([\text{area of albumin immunoreactivity}]/[\text{total region area}]) \times 100$. The "area of albumin immunoreactivity" was the count of pixels with an intensity greater than the pixel intensity threshold for that region, while the "total region area" was the number of pixels inside the drawn region. The threshold of each section was the mean pixel intensity of the reference region plus three standard-deviations. If this value resulted in selection of >2% of the pixels from the reference region, the threshold was adjusted to a value that selects <2% of the pixels in the reference region. An average of two technical replicates was obtained for each region mean pixel intensity and percent area of albumin immunostaining for further group comparison and statistical analyses.

2.7. Statistical analysis

The outcomes for CE-MRI were 1) region-specific standard deviation

of voxel intensities, 2) percent change in region-specific signal intensity from baseline (pre-contrast scan), and 3) number of region-specific voxels exceeding a threshold of percent change from baseline. The threshold used to determine the later analysis values was determined by summarizing the voxel intensity data in the regions of interest in the VEH animals and identifying the 85th percentile in these regions. The average 85th percentile across regions (15%) was used, but sensitivity analyses also evaluated 10% and 20% as a threshold and results were similar. Additional outcomes were derived from the frames of the DCE-MRI by calculating the signal intensity difference or percent change from baseline, and results were similar. Two approaches were used: the first captured AUC and was measured by summing the values across frames ending at 378 s to 1386 s; the second utilized the frame-level data to assess slopes across frames for the two outcomes. For all outcomes, mixed effects models, including animal-specific random effects, were fit to assess differences between exposure groups (DFP vs. VEH). This approach can model all available data for each animal regardless of the number and spacing of assessments and despite missing outcome data at some time points. Therefore, not all animals needed to be imaged at every time point. Primary factors of interest included exposure (DFP, VEH), brain region (PRC, AMY, HIP, THA, and SMC) and time point (6 hPE, 1, 3, 7 DPE). Interactions between factors (exposure, region, time point, and DCE-MRI change over frames) were considered, and the best model was chosen using Akaike Information Criterion (AIC). All outcomes were transformed using the natural logarithm to better meet the assumptions of the model; percent change from baseline was first shifted by 10 prior to taking the natural logarithm to make all values greater than zero.

Outcomes for IHC are region-specific mean intensity and percent albumin labeling. Mixed effects models, including animal-specific random effects, were fit to assess differences between exposure groups. Primary factors of interest included exposure (DFP, VEH), brain region (PRC, AMY, HIP, THA, and SMC) and time point (6 hPE, 1, 3, 7 DPE). Interactions between the factors (exposure, region, time point) were considered, and the best model was chosen using AIC. All outcomes were transformed using the natural logarithm to better meet the assumptions of the model; percent albumin labeling was first shifted by 0.1 prior to taking the natural logarithm to account for those with zero albumin labeling.

Results for the CE-MRI and IHC outcomes are presented as geometric mean ratios (GMR) between exposure groups for the log-transformed outcomes. Contrasts for differences between exposure groups, either overall or by region and time point, were constructed and tested using a Wald test. The Benjamini-Hochberg false discovery rate (FDR) was used within an outcome measure to account for multiple comparisons. Point estimates of the GMR and 95% confidence intervals are presented in the figures. When the confidence interval for the GMR includes 1.0, there is no statistical evidence of a difference between groups.

Spearman correlations and 95% confidence intervals for each brain region (PRC, AMY, HIP, THA, and SMC) were obtained for average seizure scores (initial, 0–40 min; and total, 0–240 min), and MRI metrics (mean and SD of percent change in signal intensity, percent tissue with signs of BBB impairment, and AUC of time-intensity curves of DCE-MRI) at the earliest imaging time point for each animal ($n = 25$), or average seizure scores (initial and total), and IHC metrics (mean intensity and area of albumin immunostaining; $n = 45$ –49). The same correlation calculation was obtained for MRI metrics at the time point of brain collection and its respective IHC, and included 6 hPE ($n = 9$), 3 DPE ($n = 4$), and 7 DPE ($n = 5$). All analyses were performed using SAS software, version 9.4, and alpha was set at 0.05.

3. Results

3.1. Acute DFP intoxication induced robust seizure behavior

To evaluate BBB integrity and seizure behavior following acute DFP

intoxication, forty-eight adult male rats were acutely intoxicated with DFP as shown in Fig. 1A. Seizure behavior was scored using a modified Racine scale (Fig. 1B) (Deshpande et al., 2010). Of the 48 DFP-intoxicated animals, 9 (18.8%) died as a consequence of DFP intoxication. Of the initial 48 rats, 2 (4.2%) presented an initial average seizure score during the first 40 min post-exposure prior to MDZ treatment that was lower than 2.5, indicating that they did not experience SE. These two animals were excluded from subsequent BBB impairment analyses; however, albumin leakage was evaluated in one of them through IHC and these data were included in the correlation calculation between seizure scores and magnitude of BBB impairment measured by albumin IHC. Of the remaining 37 rats included in the study, 2 died immediately after *in vivo* imaging acquisition, therefore their brains were not collected for IHC analysis due to potential post-mortem alterations, but the MRI scans were included in the BBB impairment analyses (Fig. 1C). All animals included in the study reached and maintained seizure scores ≥ 3 within the initial 20 min post-DFP exposure, until administered MDZ at 40 min post-exposure, when the average behavioral seizure scores decreased to ≤ 2 (Fig. 1D).

For the VEH group, a total of 22 rats were randomly distributed among the four time points: 6 hPE ($n = 4$, with MRI and IHC analysis), 1 DPE ($n = 8$, 4 with MRI only, and 4 with IHC only), 3 DPE ($n = 5$, 1 with MRI only, 1 with IHC only, and 3 with both), and 7 DPE ($n = 8$, 4 with

MRI only, and 4 with IHC only). Four rats were imaged longitudinally at 1 and 3 DPE.

3.2. CE-MRI revealed BBB impairment following acute DFP intoxication

Following DFP-induced SE, BBB impairment was examined *in vivo*. First, we assessed BBB impairment through high spatial-resolution MRI, pre- and post-contrast delivery. Parametric maps of percent change in signal intensity after *i.v.* administration of gadobenate dimeglumine (Gd) contrast agent (post-contrast scan) compared to baseline (pre-contrast scan) revealed marked, localized hyperintensity on scans of DFP-intoxicated animals, indicating infiltration of Gd into the brain parenchyma (Fig. 2A). Regional analyses of these parametric maps demonstrated BBB impairment was not ubiquitous throughout the brain, but instead was localized in specific regions and varied according to time post-DFP exposure. Quantification of regional mean percent change in signal intensity following Gd administration indicated DFP-exposed rats had greater BBB permeability to Gd compared to vehicle (VEH) animals ($P < 0.05$) in the piriform cortex (PRC) at all time points studied and in the amygdala (AMY), thalamus (THA), hippocampus (HIP), and somatosensory cortex (SMC) at 1 DPE (Fig. 2B and S2). Because of the possibility of restricted spatial localization of BBB impairment, intra-region heterogeneity was assessed by calculating the standard

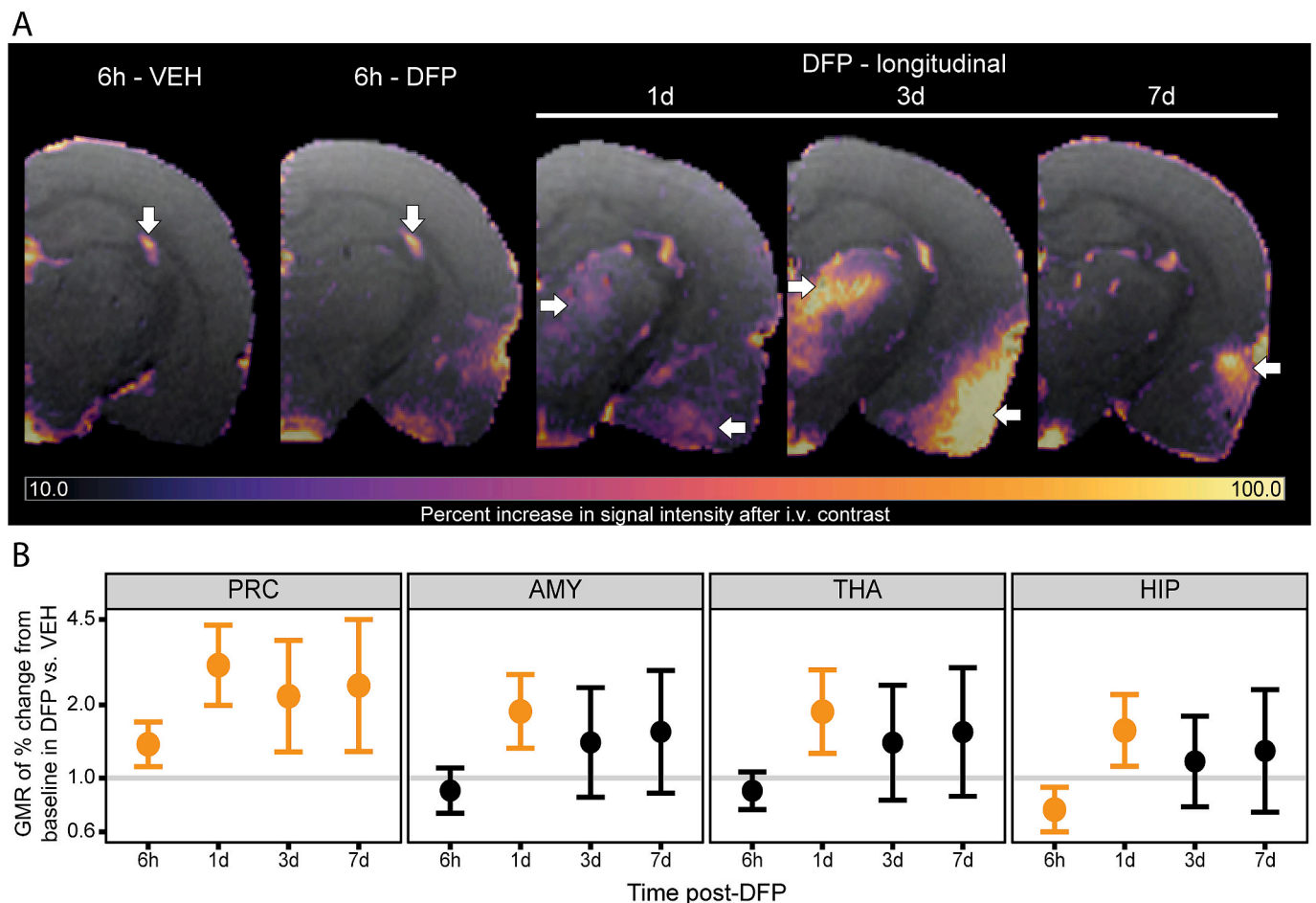


Fig. 2. Contrast-enhanced MRI revealed increased BBB permeability following acute DFP intoxication. T₁-weighted MRI scans were acquired before and after gadobenate dimeglumine (Gd) injection in DFP and vehicle control (VEH) rats at multiple time points post-DFP. (A) Representative parametric maps of the percent signal change after Gd injection (post-contrast scan) relative to baseline (pre-contrast scan). Down arrows indicate Gd distribution in lateral ventricles; left arrows, Gd in piriform cortex (PRC) and amygdala (AMY); right arrows, Gd in thalamus (THA). (B) Geometric mean ratio (GMR) with 95% confidence interval (CI) of the mean change in signal intensity from baseline curves in the PRC, AMY, THA, and hippocampus (HIP) of DFP ($n = 5-8$ per time point) vs. VEH ($n = 4$ per time point) rats (raw values and distribution are displayed in supplemental fig. S2). Mixed effects models were used for the statistical analysis. Orange bars indicate significant differences between DFP and VEH; if 95% CIs lie above 1.0, values are significantly increased in DFP vs. VEH; if CIs lie below 1.0, values are significantly reduced in DFP vs. VEH.

deviation (SD) of the voxel-wise percent change in signal intensity after Gd administration. This SD was used to detect focal points of hyperintensity within each region that may not have been captured by the regional mean percent change in signal intensity. Histograms of the percent change in total voxel count from baseline in the DFP and VEH groups (Fig. S3 and S4) represent the contrast found between these two groups. DFP-intoxicated animals had higher SD compared to VEH ($P < 0.05$) that did not vary by time point or region-specific volume of interest (VOI; Fig. S5A), indicating focal areas of Gd leakage in the DFP group throughout all VOIs and time points assessed. Furthermore, the percent of tissue with signs of Gd leakage ($> 15\%$ of change from baseline) was significantly higher in DFP-intoxicated animals relative to VEH ($P < 0.05$) at 6 hPE in the SMC, at 1 DPE for all five VOIs, and at 7 DPE in the PRC and SMC (Fig. S5B).

A second experimental method employed was high temporal-resolution dynamic contrast-enhanced (DCE) MRI. The steady leakage of contrast agent into brain parenchyma over the course of 20 min of Gd

infusion was evaluated by DCE-MRI scans (Fig. 3A) as a confirmatory analytical method. Analysis of regional time-intensity curves (Fig. S6 and S7) revealed DFP-intoxicated animals had significant Gd leakage across the BBB compared to VEH ($P < 0.05$), as indicated by a steeper positive slope of the percent change from baseline curve in the SMC at 1 DPE and in the PRC and AMY at 1, 3, and 7 DPE (Fig. 3B and S8A). At 6 hPE, in the THA, VEH animals exhibited a slightly steeper slope than DFP ($P < 0.05$) that was attributed to low variability of the measured data, resulting in a GMR with narrow 95% confidence interval (0.988 ± 0.009). BBB impairment caused by DFP intoxication was also reflected by the area under the curve (AUC) of the regional time-intensity curves (Fig. S8B), with increased Gd leakage in DFP-intoxicated animals relative to VEH in the PRC at 6 hPE and in all five VOIs at 1 and 3 DPE ($P < 0.05$). Altogether, these data demonstrated continuous leakage of Gd into the identified brain regions during the 20 min of Gd infusion, which only occurs when BBB is compromised.

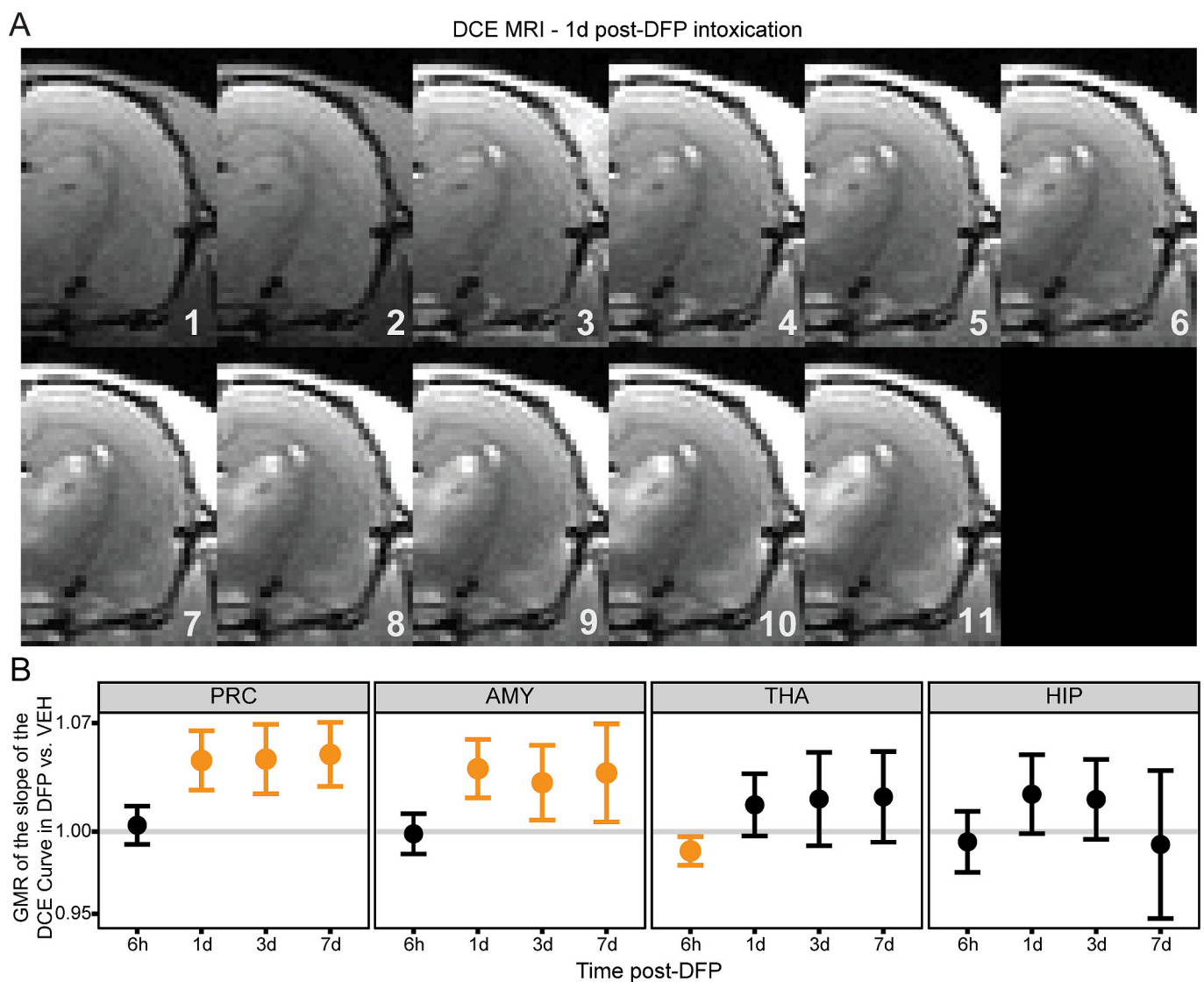


Fig. 3. Dynamic contrast-enhanced (DCE) MRI identified increased BBB permeability after acute DFP intoxication. (A) T₁-weighted DCE scans illustrate hyperintense lesions where i.v. injected contrast (Gd) extravasated into the brain parenchyma. Two initial scans (1,2) were acquired before the start of Gd infusion, and nine subsequent scans were obtained (3–11), spaced 126 s apart, from the start (3) until the end of Gd infusion (11). (B) Geometric mean ratio (GMR) with 95% confidence interval (CI) of the slope of the time-intensity curves in the piriform cortex (PRC), amygdala (AMY), thalamus (THA), and hippocampus (HIP) of DFP (n = 5–8 per time point) vs. VEH (n = 4 per time point) rats (raw values and distribution are displayed in supplemental fig. S6 and S7). Mixed effects models were used for the statistical analysis. Orange bars indicate significant differences between DFP and VEH; if 95% CIs lie entirely above 1.0, values are significantly increased in DFP vs. VEH; if CIs lie below 1.0, values are significantly reduced in DFP vs. VEH.

3.3. IHC analysis corroborated CE-MRI data indicating DFP-induced BBB impairment

Taking into consideration that MRI is a less sensitive mode of analysis compared to ex vivo immunoassays, confirmatory IHC was employed as a secondary method to verify BBB impairment through extravasation of endogenous serum albumin into the brain parenchyma, which is not expected in healthy animals with an intact BBB. Following acute DFP intoxication, serum albumin was detected by IHC using a fluorescent-tagged antibody (Fig. 4A) and quantified as the mean regional fluorescence intensity (Fig. S9) and percent regional area of albumin immunoreactivity (Fig. S10). These data revealed time- and region-dependent BBB impairment. The mean regional signal intensity of albumin immunofluorescence indicated leakage of serum albumin into the brain parenchyma of DFP-exposed animals ($P < 0.05$) in the PRC, AMY, and THA at all time points evaluated, with the exception of the PRC at 6 hPE, in the HIP at 1 and 3 DPE, and in the SMC at 3 DPE (Fig. 4B, and Fig. S11A). The percent regional area immunostained for albumin similarly indicated increased levels of leakage in the brain parenchyma of DFP-intoxicated animals compared to VEH ($P < 0.05$), with a greater area of albumin deposition observed in the PRC, AMY,

and THA at all time points but no significant difference between groups found in the HIP and SMC at any time point (Fig. S11B).

Spatial overlap between MRI and albumin IHC characterizations of BBB leakage was evident (Fig. 5). Positive correlations ($P < 0.05$) were observed in the PRC when comparing all outcomes of MRI quantification with IHC, in the AMY for all MRI metrics compared to the area of albumin immunostaining and for SD of percent change in signal intensity compared to mean intensity of albumin immunostaining, and in the HIP and SMC when comparing the AUC of the time-intensity curve with the mean intensity of albumin immunostaining. No significant correlation was detected in the THA (Tables 1, and Supplemental Table 1–3). The similar outcomes in the two methodologies for BBB impairment assessment and the largely positive correlation between them, particularly in the regions presenting greater BBB impairment, reinforce confidence in our observations.

3.4. The magnitude of BBB impairment was positively correlated with seizure scores

Different severities of BBB impairment could be observed across the DFP-intoxicated animals. Since variable behavioral seizure scores were

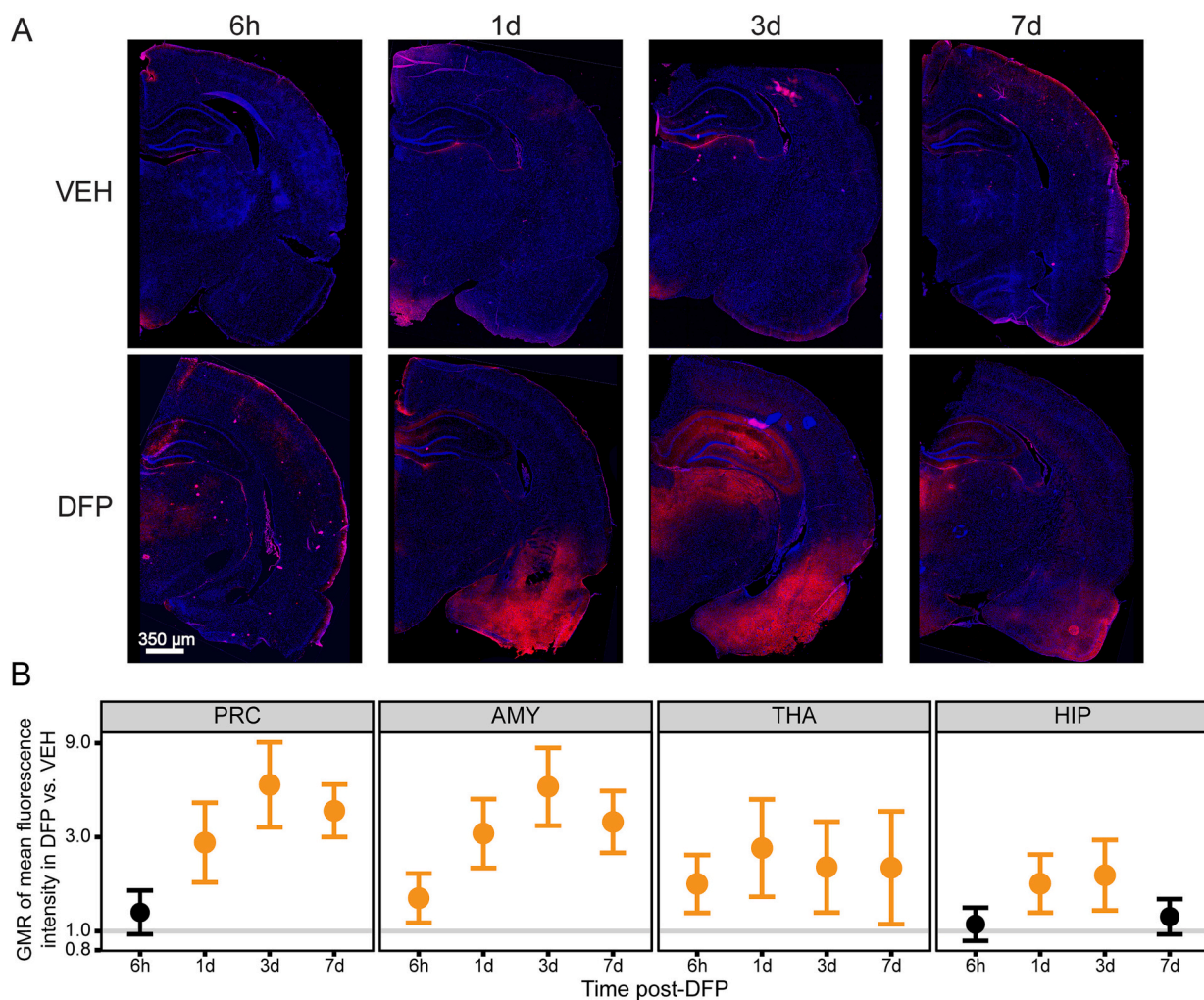


Fig. 4. Acute DFP intoxication caused leakage of serum albumin into the brain parenchyma. (A) Representative images of brains from DFP and vehicle control (VEH) rats immunostained for albumin (red) and counterstained with DAPI (blue) to identify cell nuclei. (B) Geometric mean ratio (GMR) with 95% confidence interval (CI) of the mean intensity of albumin immunostaining in the piriform cortex (PRC), amygdala (AMY), thalamus (THA), and hippocampus (HIP) of DFP ($n = 7-8$ per time point) vs. VEH ($n = 4-5$ per time point) rats (raw values and distribution are displayed in supplemental fig. S9). Mixed effects models were used for the statistical analysis. Orange bars indicate significant differences between DFP and VEH; if 95% CIs lie above 1.0, values are significantly increased in DFP vs. VEH; if CIs lie below 1.0, values are significantly reduced in DFP vs. VEH. Scale bar, 350 μm . (For interpretation of the references to colour in this figure legend, the reader is referred to the web version of this article.)

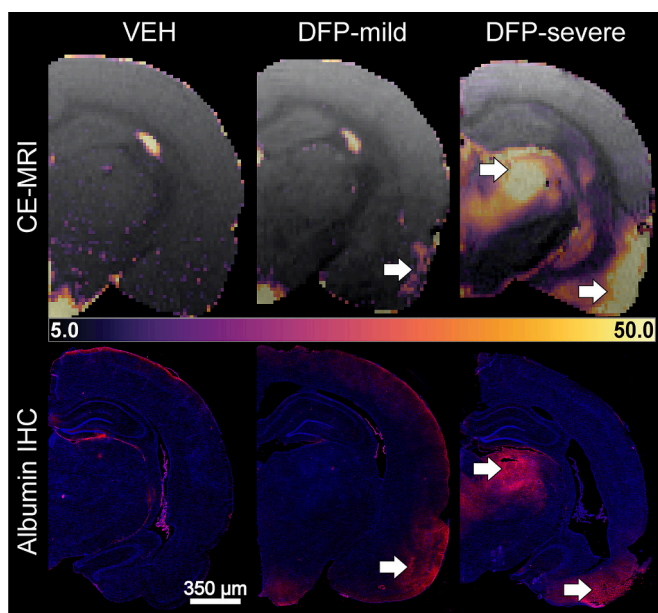


Fig. 5. Spatial association between contrast-enhanced magnetic resonance imaging (CE-MRI) and albumin immunohistochemistry (IHC). Representative subject- and time-matched MRI (top row) and fluorescent micrographs of serum albumin (red) immunoreactivity (bottom row) in vehicle (VEH) and DFP-exposed rats that experienced mild vs. severe BBB impairment. Arrows indicate spatial concordance of increased MRI signal intensity, indicative of contrast leakage, and albumin immunoreactivity in the brain parenchyma. Scale bar, 350 μ m. (For interpretation of the references to colour in this figure legend, the reader is referred to the web version of this article.)

Table 1

Spearman correlation^a between the area under the curve (AUC) of the time-intensity curve from dynamic contrast enhanced-magnetic resonance imaging (DCE-MRI) and albumin immunohistochemistry metrics.

Brain region	AUC of DCE-MRI curves vs. Mean pixel intensity of albumin staining		AUC of DCE-MRI curves vs. % Area of albumin immunoreactivity	
	ρ (95% CI)	P-value	ρ (95% CI)	P-value
PRC	0.66 (0.27–0.87)	0.003	0.65 (0.25–0.86)	0.004
AMY	0.40 (–0.07–0.73)	0.10	0.55 (0.11–0.81)	0.02
THA	0.45 (–0.02–0.76)	0.06	0.29 (–0.21–0.66)	0.25
HIP	0.47 (0.001–0.77)	0.049	0.03 (–0.44–0.49)	0.90
SMC	0.48 (0.01–0.77)	0.04	–0.14 (–0.57–0.35)	0.58

^a The correlation was calculated for each separate brain region and the table indicates a positive correlation if the Rho (ρ) value with the 95% confidence interval (CI) are >0 or a negative correlation if the values are <0 ($n = 17–18$). Statistically significant correlations are bolded (P -value <0.05).

observed during the 4 h post-DFP injection, we examined whether there was an association between the severity of seizure behavior and the extent of BBB impairment. Spearman correlations between mean seizure scores (initial and total) and BBB leakage metrics (CE-MRI and albumin IHC) were calculated for each region of interest (ROI)/VOI. The total average seizure scores (0–240 min post-DFP injection) were positively correlated with BBB impairment metrics, including AUC of the time-intensity curve in the PRC, AMY, HIP, and SMC (Table 2); mean percent change in signal intensity in the SMC (Supplemental Table 4); SD of the percent change in signal intensity in all brain regions (Supplemental Table 5); percent of tissue with evidence of Gd leakage in the SMC (Supplemental Table 6); mean intensity of albumin staining in all brain regions (Table 3); and area of albumin staining in the PRC, AMY, and THA (Supplemental Table 7). Initial average seizure scores (0–40

Table 2

Spearman correlation^a between the area under the curve (AUC) for the time-intensity curve from the dynamic contrast-enhanced magnetic resonance imaging (DCE-MRI) and seizure behavior.

Brain regions:	AUC of DCE-MRI curves vs. Initial average seizure score (0–40 min)		AUC of DCE-MRI curves vs. Total average seizure score (0–240 min)	
	ρ (95% CI)	P-value	ρ (95% CI)	P-value
PRC	0.56 (0.22–0.78)	0.003	0.74 (0.49–0.88)	<0.001
AMY	0.28 (–0.13–0.61)	0.17	0.56 (0.21–0.78)	0.003
THA	0.19 (–0.22–0.55)	0.36	0.36 (–0.04–0.66)	0.08
HIP	0.23 (–0.18–0.58)	0.26	0.41 (0.02–0.69)	0.04
SMC	0.33 (–0.07–0.64)	0.10	0.61 (0.28–0.81)	<0.001

^a The correlation was calculated for each separate brain region and the table indicates a positive correlation if the Rho (ρ) value with the 95% confidence interval (CI) are >0 or a negative correlation if the values are <0 ($n = 25$). Statistically significant correlations are bolded (P -value <0.05).

Table 3

Spearman correlation^a between mean intensity of albumin immunostaining and seizure behavior.

Brain regions:	Mean pixel intensity of albumin staining vs. Initial average seizure score (0–40 min)		Mean pixel intensity of albumin staining vs. Total average seizure score (0–240 min)	
	ρ (95% CI)	P-value	ρ (95% CI)	P-value
PRC	0.48 (0.22–0.68)	<0.001	0.71 (0.52–0.83)	<0.001
AMY	0.57 (0.34–0.73)	<0.001	0.76 (0.61–0.86)	<0.001
THA	0.45 (0.20–0.65)	<0.001	0.70 (0.53–0.82)	<0.001
HIP	0.39 (0.13–0.61)	0.005	0.62 (0.41–0.77)	<0.001
SMC	0.29 (0.01–0.53)	0.04	0.47 (0.22–0.67)	<0.001

^a The correlation was calculated for each separate brain region and the table indicates a positive correlation if the Rho (ρ) value with the 95% confidence interval (CI) are >0 or a negative correlation if the values are <0 ($n = 45–49$). Statistically significant correlations are bolded (P -value <0.05).

min post-DFP injection) were also positively correlated with the AUC of the time-intensity curve in the PRC ($P < 0.05$; Table 2) but negatively correlated ($P < 0.05$) for the mean percent change in signal intensity in the THA (Supplemental Table 4). For the albumin IHC metrics ($n = 45–49$), initial seizure score was positively correlated with mean intensity of albumin staining in all regions (Table 3) and with area of albumin staining in the PRC and AMY (Supplemental Table S7). Overall, these data provided evidence of a positive correlation between seizure severity and BBB dysfunction, with more BBB leakage associated with more severe seizure behavior.

4. Discussion

While previous experimental studies have demonstrated that acute OP intoxication can cause BBB breakdown (Abdel-Rahman et al., 2002; Bar-Klein et al., 2017; Rojas et al., 2022; Rojas et al., 2021), a detailed characterization of the duration, magnitude, and spatial distribution of BBB impairment has been lacking, which represents the critical data gap addressed in this study. Using a human-relevant rat model of acute DFP intoxication with delayed administration of standard of care treatment for OP-induced SE, we observed increased BBB permeability over the first week post-exposure as detected using in vivo MRI and ex vivo albumin IHC. Compromised BBB integrity was detected at 6 hPE and at 1, 3 and 7 DPE, which corresponds to the epileptogenic period following acute OP intoxication (De Araujo Furtado et al., 2010; de Araujo Furtado et al., 2012; Guignet et al., 2020; Shrot et al., 2014). The most severe and persistent BBB impairment was observed in the PRC and AMY, while the THA exhibited moderate but persistent BBB leakage. The HIP and SMC

showed the least severe and most transient degradation of BBB integrity. This spatial distribution of BBB impairment coincides with brain regions previously reported to exhibit progressive neurodegenerative and neuroinflammatory responses in this same model (Guignet et al., 2020; Hobson et al., 2019; Hobson et al., 2017), suggesting an association among these pathological processes.

Our observations of BBB impairment following acute DFP intoxication are broadly consistent with previous studies of experimental models of acute OP intoxication (Abdel-Rahman et al., 2002; Bar-Klein et al., 2017; Rojas et al., 2022; Rojas et al., 2021), including two studies from the same research group that used a rat model of acute DFP intoxication similar to the one used here. In both prior DFP studies, BBB permeability was assessed using western blot to quantify albumin in cortical tissue. One study found significant BBB impairment at 4 DPE (Rojas et al., 2021), which was the only time point examined, while the other observed significantly increased BBB permeability at 3 hPE, but not at 1 or 2 DPE (Rojas et al., 2022). The major difference between these studies is that in the former, DFP-intoxicated rats were not administered any anti-seizure medication post-exposure, and thus experienced intense seizure activity lasting >1 h (Rojas et al., 2021), while in the latter, DFP-intoxicated rats were administered urethane at 1 hPE, which effectively terminated seizure activity (Rojas et al., 2022). Thus, the likely explanation for the discrepancy in the persistence of DFP-induced BBB breakdown between these two studies is the difference in seizure duration, with the animals that experienced a longer period of seizure activity exhibiting more persistent BBB impairment. BBB damage has also been reported in studies of animals acutely intoxicated with OPs other than DFP, specifically sarin and paraoxon. Similar to our findings, BBB impairment was observed at 1 DPE in a rat model of acute sarin intoxication (Abdel-Rahman et al., 2002), as determined by brain uptake of [³H]-hexamethonium iodide, and at 2 and 7 DPE in rats acutely intoxicated with paraoxon (Bar-Klein et al., 2017), as determined using CE-MRI, albumin IHC and extravasation of i.v. injected Evans blue into brain tissue. Consistent with our findings, the studies of rats acutely intoxicated with paraoxon reported increased BBB permeability in the PRC and AMY at 2 DPE. However, in contrast to our observations, at 7 DPE, BBB leakage was present only in the neocortex and striatum of the paraoxon-intoxicated rats (Bar-Klein et al., 2017). Variation in the spatial profile of BBB damage between the paraoxon and DFP models may reflect distinct OP toxicity profiles, which are known to differ between OPs despite comparable inhibition of acetylcholinesterase (Rojas et al., 2021). Collectively, these data demonstrate that compromised BBB integrity following acute intoxication is a shared property of diverse OPs, but the spatiotemporal profile and/or severity of BBB impairment may vary depending on the OP and/or the duration of seizure activity.

Consistent with the hypothesis that seizure activity influences BBB damage, we identified a positive correlation between the behavioral seizure score and numerous metrics of BBB leakage in DFP-intoxicated animals. The strongest association was found in the PRC and AMY, which are brain regions previously demonstrated to be among the most severely damaged in our rat model of acute DFP intoxication (Guignet et al., 2020; Hobson et al., 2019; Hobson et al., 2017; Sisó et al., 2017). These observations are in accord with the prevailing hypothesis that seizure activity is the predominant cause of the neuropathology observed after acute OP intoxication (McDonough Jr and Shih, 1997; Tanaka et al., 1996). However, it should be noted that acute DFP intoxication has been shown to cause significant neuropathology in the rat brain in the absence of SE (González et al., 2020). Additionally, in juvenile (25–30 d), but not adult rats, intoxication with paraoxon at a dose that caused neither significant cholinergic toxicity nor seizures significantly increased BBB permeability (Song et al., 2004). Thus, while there is a positive correlation between seizure severity and the extent of BBB damage, suggesting seizures are a primary determinant of BBB impairment (Löscher, 2020; Obermeier et al., 2013; Rempel et al., 2018), a role for seizure-independent mechanism(s) in BBB impairment cannot be ruled out.

Two key questions not addressed in this study are: 1) is BBB impairment predictive of individuals at high risk for developing SRS after acute OP intoxication; and 2) is BBB impairment causally linked to OP-induced SRS. Consistent with the hypothesis that increased BBB permeability is a biomarker and/or cause of SRS (Swissa et al., 2019), we observed significant BBB impairment in brain regions implicated in epileptogenesis (Breuer et al., 2017; Dedeurwaerdere et al., 2012; Russmann et al., 2017) during the latent period preceding the onset of SRS. Also consistent with this hypothesis, extravasation of macromolecules (albumin, fibrinogen), small polar molecules (ions, metabolic products), and immune cells from the blood into the brain parenchyma due to BBB impairment have been shown to trigger seizures (Cserr et al., 1981; Obermeier et al., 2013). Earlier studies demonstrated that treatment with isoflurane anesthesia or losartan to terminate SE 30 min after initiation of paraoxon-induced SE significantly decreased BBB leakage during the first week post-exposure and prevented the onset of SRS (Bar-Klein et al., 2017). These findings suggest that BBB impairment may be a predictive biomarker of SRS and hint at a causal relationship, a hypothesis supported by clinical observation that individuals with new onset of refractory SE presented with greater BBB permeability measured by DCE-MRI than either patients with encephalitis without SE or healthy subjects (Li et al., 2023). However, it is not possible to determine whether the treatment with isoflurane and losartan mitigated SRS via BBB stabilization or diminution of SE, the latter also mediating protective effects on the BBB. Moreover, BBB leakage is a characteristic neuropathology of many chronic neurodegenerative diseases in which the individual is more susceptible to seizures, such as Alzheimer's disease (Yamazaki and Kanekiyo, 2017). These observations suggest that if BBB impairment is causally linked to SRS, various factors, such as the severity and spatiotemporal profile of BBB damage, and perhaps specific molecular and/or mechanistic changes of the neurovascular unit (NVU), determine whether BBB impairment leads to SRS (Löscher, 2020). Knowledge of the spatiotemporal map of BBB disruption, as established in this study for the rat model of acute DFP intoxication, is essential to answer these questions.

In addition to not addressing causal relationships between BBB impairment and seizures, this study was limited by the fact that while CE-MRI and serum albumin IHC are sensitive methods for detecting BBB leakage (Di Biase et al., 2021; Krueger et al., 2015), neither provides information regarding molecular or cellular damage to the NVU that comprises the BBB. However, our methods were able to detect serum albumin extravasation into the brain parenchyma, which indirectly identifies molecular and cellular dysfunction, specifically astrocytic and neuronal function and dysregulation of the NVU through activation of TGFβ signaling (Kim et al., 2017; Luo, 2022; Senatorov Jr et al., 2019). Addressing this data gap will be important for designing targeted strategies for protecting BBB integrity following acute OP intoxication, which is only possible after the BBB impairment profile is clearly determined.

Another potential limitation of this study is that serum albumin IHC does not provide precise temporal resolution of BBB leakage given its estimated half-life clearance from brain parenchyma of up to 18 h (Cserr et al., 1981; Hladky and Barrand, 2018). However, IHC detection of albumin is a widely accepted and sensitive technique for defining the spatial pattern of BBB impairment (Krueger et al., 2015). In addition, the parallel use of CE-MRI provides exquisite spatiotemporal resolution of BBB impairment (Di Biase et al., 2021).

The heterogeneity of the neuropathological response observed in the rat model of acute DFP intoxication is another limitation of this study (Guignet et al., 2020; Hobson et al., 2019; Hobson et al., 2017; Sisó et al., 2017). To mitigate this challenge, inclusion criteria based on behavior seizure scores (> 2.5 in the initial 40 min post-exposure to DFP) were applied. Nonetheless, this factor could not be entirely controlled, as evidenced by the high variability of the BBB metrics observed in the DFP group. Lastly, this study used only male rats, thus decreasing the heterogeneity of the studied population. However, future

investigations will include females to determine whether sex influences BBB impairment following acute OP intoxication.

5. Conclusion

Our findings suggest that further investigation of BBB impairment as a biomarker and therapeutic target for OP-induced SRS is warranted, but success depends on a comprehensive understanding of the spatiotemporal profile of BBB impairment, as generated here. Identifying the molecular and cellular components of the NVU that are altered following acute OP intoxication, which is the focus of ongoing studies, is the next step to advance this research. Collectively, these data will inform the pharmacological target and therapeutic window for stabilizing BBB function following acute OP intoxication (Li et al., 2021) with the long-term goal of identifying adjunct therapies that can be administered at delayed times post-exposure to mitigate spontaneous recurrent seizures and possibly other chronic neurological morbidities associated with acute OP intoxication.

Funding source

This work was supported by the National Institute of Neurological Disorders and Stroke CounterACT program grant numbers NS079202 and NS127758 (P.J.L.); the 2022-2023 Lodric Maddox Graduate Fellowship from the UC Davis School of Veterinary Medicine (PNB); and the 2020-2023 ARCS Foundation Northern California Scholar (PMA). The sponsors were not involved in the study design, the collection, analysis, and interpretation of data, in the writing of the report or in the decision to submit the paper for publication.

CRedit authorship contribution statement

Pedro N. Bernardino: Conceptualization, Methodology, Investigation, Data curation, Visualization, Validation, Project administration, Supervision, Writing – original draft, Writing – review & editing. **Brad A. Hobson:** Conceptualization, Methodology, Investigation, Data curation, Visualization, Writing – original draft, Writing – review & editing. **Sydney L. Huddleston:** Investigation, Visualization. **Peter M. Andrew:** Investigation, Visualization. **Jeremy A. MacMahon:** Investigation, Visualization. **Naomi H. Saito:** Data curation, Formal analysis, Visualization. **Valerie A. Porter:** Visualization. **Donald A. Bruun:** Investigation. **Danielle J. Harvey:** Data curation, Formal analysis, Visualization, Writing – original draft. **Joel R. Garbow:** Methodology, Writing – original draft. **Angie Gelli:** Methodology, Validation, Project administration, Supervision, Writing – original draft. **Abhijit J. Chaudhari:** Methodology, Validation, Project administration, Supervision, Writing – original draft. **Pamela J. Lein:** Conceptualization, Methodology, Funding acquisition, Validation, Project administration, Supervision, Writing – review & editing.

Declaration of Competing Interest

None.

Data availability

Data and materials will be made available upon reasonable request to the corresponding author.

Acknowledgments

We thank Suzette Smiley-Jewell (UC Davis) for providing feedback on early versions of this manuscript.

Appendix A. Supplementary data

Supplementary data to this article can be found online at <https://doi.org/10.1016/j.nbd.2023.106316>.

References

- Abbott, N.J., Patabendige, A.A., Dolman, D.E., Yusof, S.R., Begley, D.J., 2010. Structure and function of the blood–brain barrier. *Neurobiol. Dis.* 37, 13–25.
- Abdel-Rahman, A., Shetty, A., Abou-Donia, M., 2002. Acute exposure to sarin increases blood–brain barrier permeability and induces neuropathological changes in the rat brain: dose–response relationships. *Neuroscience*. 113, 721–741.
- Bar-Klein, G., Lublinsky, S., Kamintsky, L., Noyman, I., Veksler, R., Dalipaj, H., Senatorov, V.V., Swissa, E., Rosenbach, D., Elazary, N., 2017. Imaging blood–brain barrier dysfunction as a biomarker for epileptogenesis. *Brain*. 140, 1692–1705.
- Bird, S., Traub, S., Grayzel, J., 2014. Organophosphate and carbamate poisoning. *UpToDate*. 14, 339.
- Breuer, H., Meier, M., Schneefeld, S., Härtig, W., Wittneben, A., Märkel, M., Ross, T.L., Bengel, F.M., Bankstahl, M., Bankstahl, J.P., 2017. Multimodality imaging of blood–brain barrier impairment during epileptogenesis. *J. Cereb. Blood Flow Metab.* 37, 2049–2061.
- Bruun, D.A., Guignet, M., Harvey, D.J., Lein, P.J., 2019. Pretreatment with pyridostigmine bromide has no effect on seizure behavior or 24 hour survival in the rat model of acute diisopropylfluorophosphate intoxication. *Neurotoxicology*. 73, 81–84.
- Cserr, H., Cooper, D., Suri, P., Patlak, C., 1981. Efflux of radiolabeled polyethylene glycols and albumin from rat brain. *American J. Physiol.-Renal Physiol.* 240, F319–F328.
- Dadas, A., Janigro, D., 2019. Breakdown of blood brain barrier as a mechanism of post-traumatic epilepsy. *Neurobiol. Dis.* 123, 20–26.
- De Araujo Furtado, M., Lumley, L.A., Robison, C., Tong, L.C., Lichtenstein, S., Yourick, D. L., 2010. Spontaneous recurrent seizures after status epilepticus induced by soman in Sprague-Dawley rats. *Epilepsia*. 51, 1503–1510.
- de Araujo Furtado, M., Rossetti, F., Chanda, S., Yourick, D., 2012. Exposure to nerve agents: from status epilepticus to neuroinflammation, brain damage, neurogenesis and epilepsy. *Neurotoxicology*. 33, 1476–1490.
- Dedeurwaerdere, S., Callaghan, P.D., Pham, T., Rahardjo, G.L., Amhaoul, H., Berghofer, P., Quinlivan, M., Mattner, F., Loc'h, C., Katsifis, A., 2012. PET imaging of brain inflammation during early epileptogenesis in a rat model of temporal lobe epilepsy. *EJNMMI Res.* 2, 1–13.
- Deshpande, L.S., Carter, D.S., Blair, R.E., DeLorenzo, R.J., 2010. Development of a prolonged calcium plateau in hippocampal neurons in rats surviving status epilepticus induced by the organophosphate diisopropylfluorophosphate. *Toxicol. Sci.* 116, 623–631.
- Deshpande, L.S., Blair, R.E., Phillips, K.F., DeLorenzo, R.J., 2016. Role of the calcium plateau in neuronal injury and behavioral morbidities following organophosphate intoxication. *Ann. N. Y. Acad. Sci.* 1374, 176–183.
- Dhir, A., Wu, C.Y., Rogawski, M.A., 2021. Intramuscular Dose of Midazolam in Rats Producing Exposure Equivalent to Recommended Dose of Seizalám® (Midazolam Injection) in Humans, 413.
- Di Biase, M.A., Chad, J.A., Pasternak, O., 2021. Magnetic Resonance Imaging Measures of Neuroinflammation in Psychiatry. *Immuno-Psychiatry*. Springer, pp. 51–65.
- Eddleston, M., Buckley, N.A., Eyer, P., Dawson, A.H., 2008. Management of acute organophosphorus pesticide poisoning. *Lancet* 371, 597–607.
- Farrell, J.S., Wolff, M.D., Teskey, G.C., 2017. Neurodegeneration and Pathology in Epilepsy: Clinical and Basic Perspectives. *Neurodegenerative Diseases: Pathology, Mechanisms, and Potential Therapeutic Targets*, pp. 317–334.
- Gao, J., Naughton, S.X., Wulff, H., Singh, V., Beck, W.D., Magrane, J., Thomas, B., Kaidery, N.A., Hernandez, C.M., Terry, A.V., 2016. Diisopropylfluorophosphate impairs the transport of membrane-bound organelles in rat cortical axons. *J. Pharmacol. Exp. Ther.* 356, 645–655.
- González, E.A., Rindy, A.C., Guignet, M.A., Calsbeek, J.J., Bruun, D.A., Dhir, A., Andrew, P., Saito, N., Rowland, D.J., Harvey, D.J., 2020. The chemical convulsant diisopropylfluorophosphate (DFP) causes persistent neuropathology in adult male rats independent of seizure activity. *Arch. Toxicol.* 94, 2149–2162.
- Guignet, M., Dhakal, K., Flannery, B.M., Hobson, B.A., Zolkowska, D., Dhir, A., Bruun, D. A., Li, S., Wahab, A., Harvey, D.J., 2020. Persistent behavior deficits, neuroinflammation, and oxidative stress in a rat model of acute organophosphate intoxication. *Neurobiol. Dis.* 133, 104431.
- Heiss, D.R., Zehnder, D.W., Jett, D.A., Platoff, G.E., Yeung, D.T., Brewer, B.N., 2016. Synthesis and storage stability of diisopropylfluorophosphate. *J. Chemother.* 2016.
- Hill, C.E., Parikh, A.O., Ellis, C., Myers, J.S., Litt, B., 2017. Timing is everything: where status epilepticus treatment fails. *Ann. Neurol.* 82, 155–165.
- Hladky, S.B., Barrand, M.A., 2018. Elimination of substances from the brain parenchyma: efflux via perivascular pathways and via the blood–brain barrier. *Fluid. Barriers CNS.* 15, 1–73.
- Hobson, B.A., Sisó, S., Rowland, D.J., Harvey, D.J., Bruun, D.A., Garbow, J.R., Lein, P.J., 2017. From the cover: magnetic resonance imaging reveals progressive brain injury in rats acutely intoxicated with diisopropylfluorophosphate. *Toxicol. Sci.* 157, 342–353.
- Hobson, B.A., Rowland, D.J., Sisó, S., Guignet, M.A., Harmany, Z.T., Bandara, S.B., Saito, N., Harvey, D.J., Bruun, D.A., Garbow, J.R., 2019. TSPO PET using [18F] PBR111 reveals persistent neuroinflammation following acute diisopropylfluorophosphate intoxication in the rat. *Toxicol. Sci.* 170, 330–344.

- Jett, D.A., Sibrizzi, C.A., Blain, R.B., Hartman, P.A., Lein, P.J., Taylor, K.W., Rooney, A.A., 2020. A national toxicology program systematic review of the evidence for long-term effects after acute exposure to sarin nerve agent. *Crit. Rev. Toxicol.* 50, 474–490.
- Jh, J.M., Zoefel, L., McMonagle, J., Copeland, T., Smith, C., Shih, T., 2000. Anticonvulsant treatment of nerve agent seizures: anticholinergics versus diazepam in soman-intoxicated guinea pigs. *Epilepsy Res.* 1, 114Oydv.
- Kadry, H., Noorani, B., Cucullo, L., 2020. A blood–brain barrier overview on structure, function, impairment, and biomarkers of integrity. *Fluid. Barriers CNS.* 17, 1–24.
- Kapur, J., Elm, J., Chamberlain, J.M., Barsan, W., Cloyd, J., Lowenstein, D., Shinnar, S., Conwit, R., Meinzer, C., Cock, H., 2019. Randomized trial of three anticonvulsant medications for status epilepticus. *N. Engl. J. Med.* 381, 2103–2113.
- Kim, S.Y., Senatorov, V.V., Morrissey, C.S., Lippmann, K., Vazquez, O., Milikovsky, D.Z., Gu, F., Parada, I., Prince, D.A., Becker, A.J., 2017. TGF β signaling is associated with changes in inflammatory gene expression and perineuronal net degradation around inhibitory neurons following various neurological insults. *Sci. Rep.* 7, 1–14.
- Krueger, M., Bechmann, I., Immig, K., Reichenbach, A., Härtig, W., Michalski, D., 2015. Blood–brain barrier breakdown involves four distinct stages of vascular damage in various models of experimental focal cerebral ischemia. *J. Cereb. Blood Flow Metab.* 35, 292–303.
- Li, J., Zheng, M., Shimoni, O., Banks, W.A., Bush, A.I., Gamble, J.R., Shi, B., 2021. Development of novel therapeutics targeting the blood–brain barrier: from barrier to carrier. *Adv. Sci.* 8, 2101090.
- Li, H., Liu, X., Wang, R., Lu, A., Ma, Z., Wu, S., Lu, H., Du, Y., Deng, K., Wang, L., 2023. Blood-brain barrier damage and new-onset refractory status epilepticus: an exploratory study using dynamic contrast-enhanced MRI. *Epilepsia* 64, 1594–1604.
- Löscher, W., 2020. Epilepsy and alterations of the blood–brain barrier: cause or consequence of epileptic seizures or both?. In: *Handbook of Experimental Pharmacology*. Springer, pp. 331–350.
- Luo, J., 2022. TGF- β as a key modulator of astrocyte reactivity: disease relevance and therapeutic implications. *Biomedicines*. 10, 1206.
- Marchi, N., Granata, T., Ghosh, C., Janigro, D., 2012. Blood–brain barrier dysfunction and epilepsy: pathophysiologic role and therapeutic approaches. *Epilepsia*. 53, 1877–1886.
- Masson, P., 2011. Evolution of and perspectives on therapeutic approaches to nerve agent poisoning. *Toxicol. Lett.* 206, 5–13.
- McDonough Jr., J.H., Shih, T.-M., 1997. Neuropharmacological mechanisms of nerve agent-induced seizure and neuropathology. *Neurosci. Biobehav. Rev.* 21, 559–579.
- Mendes, N.F., Pansani, A.P., Carmanhães, E.R.F., Tange, P., Meireles, J.V., Ochikubo, M., Chagas, J.R., da Silva, A.V., Monteiro de Castro, G., Le Sueur-Maluf, L., 2019. The blood-brain barrier breakdown during acute phase of the pilocarpine model of epilepsy is dynamic and time-dependent. *Front. Neurol.* 10, 382.
- Mew, E.J., Padmanathan, P., Konradsen, F., Eddleston, M., Chang, S.-S., Phillips, M.R., Gunnell, D., 2017. The global burden of fatal self-poisoning with pesticides 2006–15: systematic review. *J. Affect. Disord.* 219, 93–104.
- Nation, D.A., Sweeney, M.D., Montagne, A., Sagare, A.P., D’Orazio, L.M., Pachicano, M., Sepeshband, F., Nelson, A.R., Buennagel, D.P., Harrington, M.G., 2019. Blood–brain barrier breakdown is an early biomarker of human cognitive dysfunction. *Nat. Med.* 25, 270–276.
- Obermeier, B., Daneman, R., Ransohoff, R.M., 2013. Development, maintenance and disruption of the blood–brain barrier. *Nat. Med.* 19, 1584–1596.
- Paxinos, G., Watson, C., 2006. *The Rat Brain in Stereotaxic Coordinates: Hard Cover Edition*. Elsevier.
- Profaci, C.P., Munji, R.N., Pulido, R.S., Daneman, R., 2020. The blood–brain barrier in health and disease: important unanswered questions. *J. Exp. Med.* 217.
- Rempe, R.G., Hartz, A.M., Soldner, E.L., Sokola, B.S., Alluri, S.R., Abner, E.L., Kryscio, R. J., Pekcec, A., Schlichtiger, J., Bauer, B., 2018. Matrix metalloproteinase-mediated blood-brain barrier dysfunction in epilepsy. *J. Neurosci.* 38, 4301–4315.
- Rojas, A., McCarren, H.S., Wang, J., Wang, W., Abreu-Melon, J., Wang, S., McDonough, J.H., Dingleline, R., 2021. Comparison of neuropathology in rats following status epilepticus induced by diisopropylfluorophosphate and soman. *Neurotoxicology*. 83, 14–27.
- Rojas, A., Abreu-Melon, J., Wang, S., Dingleline, R., 2022. Time-dependent neuropathology in rats following organophosphate-induced status epilepticus. *Neurotoxicology*. 91, 45–59.
- Russmann, V., Brendel, M., Mille, E., Helm-Vicidomini, A., Beck, R., Günther, L., Lindner, S., Rominger, A., Keck, M., Salvamoser, J.D., 2017. Identification of brain regions predicting epileptogenesis by serial [18F] GE-180 positron emission tomography imaging of neuroinflammation in a rat model of temporal lobe epilepsy. *NeuroImag.: Clin.* 15, 35–44.
- Senatorov Jr., V.V., Friedman, A.R., Milikovsky, D.Z., Ofer, J., Saar-Ashkenazy, R., Charbash, A., Jahan, N., Chin, G., Mihaly, E., Lin, J.M., 2019. Blood-brain barrier dysfunction in aging induces hyperactivation of TGF β signaling and chronic yet reversible neural dysfunction. *Sci. Transl. Med.* 11 eaaw8283.
- Shih, T.-M., 1990. Anticonvulsant effects of diazepam and MK-801 in soman poisoning. *Epilepsy Res.* 7, 105–116.
- Shrot, S., Ramaty, E., Biala, Y., Bar-Klein, G., Daninos, M., Kamintsky, L., Makarovsky, I., Statlender, L., Rosman, Y., Krivoy, A., 2014. Prevention of organophosphate-induced chronic epilepsy by early benzodiazepine treatment. *Toxicology*. 323, 19–25.
- Sisó, S., Hobson, B.A., Harvey, D.J., Bruun, D.A., Rowland, D.J., Garbow, J.R., Lein, P.J., 2017. Editor’s highlight: spatiotemporal progression and remission of lesions in the rat brain following acute intoxication with diisopropylfluorophosphate. *Toxicol. Sci.* 157, 330–341.
- Song, X., Pope, C., Murthy, R., Shaikh, J., Lal, B., Bressler, J.P., 2004. Interactive effects of paraoxon and pyridostigmine on blood-brain barrier integrity and cholinergic toxicity. *Toxicol. Sci.* 78, 241–247.
- Supasai, S., González, E.A., Rowland, D.J., Hobson, B., Bruun, D.A., Guignet, M.A., Soares, S., Singh, V., Wulff, H., Saito, N., 2020. Acute administration of diazepam or midazolam minimally alters long-term neuropathological effects in the rat brain following acute intoxication with diisopropylfluorophosphate. *Eur. J. Pharmacol.* 886, 173538.
- Swissa, E., Serlin, Y., Vazana, U., Prager, O., Friedman, A., 2019. Blood–brain barrier dysfunction in status epilepticus: mechanisms and role in epileptogenesis. *Epilepsy Behav.* 101, 106285.
- Tanaka, K., Graham, S., Simon, R., 1996. The role of excitatory neurotransmitters in seizure-induced neuronal injury in rats. *Brain Res.* 737, 59–63.
- Tenreiro, M., Ferreira, R., Bernardino, L., Brito, M., 2016. Cellular response of the blood-brain barrier to injury: potential biomarkers and therapeutic targets for brain regeneration. *Neurobiol. Dis.* 91, 262–273.
- Uprety, A., Kang, Y., Kim, S.Y., 2021. Blood-brain barrier dysfunction as a potential therapeutic target for neurodegenerative disorders. *Arch. Pharm. Res.* 44, 487–498.
- U.S Department of Health and Human Services. Nerve Agents, 2023. Emergency Department/Hospital Management.** https://chemm.hhs.gov/na_hospital_mmg.htm#top.
- van Lanen, R.H., Melchers, S., Hoogland, G., Schijns, O.E., Zandvoort, M.A.V., Haeren, R. H., Rijkers, K., 2021. Microvascular changes associated with epilepsy: a narrative review. *J. Cereb. Blood Flow Metab.* 41, 2492–2509.
- Van Vliet, E., Otte, W., Gorter, J., Dijkhuizen, R., Wadman, W., 2014. Longitudinal assessment of blood–brain barrier leakage during epileptogenesis in rats. A quantitative MRI study. *Neurobiol. Dis.* 63, 74–84.
- Van Vliet, E., Aronica, E., Gorter, J., 2015. Blood–brain barrier dysfunction, seizures and epilepsy. In: *Seminars in Cell & Developmental biology*, 38. Elsevier, pp. 26–34.
- Waheed, S., Sabeen, A., Ullah Khan, N., 2014. New onset refractory status epilepticus as an unusual presentation of a suspected organophosphate poisoning. *Case Rep. Emerg. Med.* 2014.
- Weissman, B.A., Raveh, L., 2008. Therapy against organophosphate poisoning: the importance of anticholinergic drugs with antiglutamatergic properties. *Toxicol. Appl. Pharmacol.* 232, 351–358.
- Yamazaki, Y., Kanekiyo, T., 2017. Blood-brain barrier dysfunction and the pathogenesis of Alzheimer’s disease. *Int. J. Mol. Sci.* 18, 1965.